Bull. Mater. Sci. (2018) 41:129
https://doi.org/10.1007/s12034-018-1635-x

Synthesis and properties of graphene and its 2D inorganic analogues with potential applications

UTTAM GUPTA, K GOPALAKRISHNAN and C N R RAO*
Chemistry and Physics of Materials Unit, New Chemistry Unit, CSIR Centre of Excellence in Chemistry, International Centre for Materials Science and Sheikh Saqr Laboratory, Jawaharlal Nehru Centre for Advanced Scientific Research, Jakkur P.O., Bangalore 560064, India
*Author for correspondence (cnrrao@jncasr.ac.in)

MS received 21 March 2018; accepted 26 April 2018; published online 21 September 2018

Abstract. Discovery of the amazing properties of graphene has aroused great interest in other 2D materials. 2D inorganic analogues of graphene such as the transition metal dichalcogenides have been investigated widely and these materials, especially MoS_2, exhibit many properties of interest. In particular, they possess properties of direct use in energy devices. In this article we review the synthesis and properties of the 2D materials of relevant transistors, sensors, photodetectors, supercapacitors and batteries as well as in oxygen reduction and hydrogen evolution reactions.

Keywords. 2D materials; energy applications; supercapacitors; Li batteries; oxygen reduction reaction; hydrogen evolution reaction.

1. Introduction

Graphene and transition metal dichalcogenides (TMDs) and such 2D layered materials exhibit fascinating properties, which can be employed for applications in transistors, sensing, energy storage and catalysis [1,2]. Graphene has exotic electronic properties, but due to its gapless nature, it cannot be used in certain electronic applications. There have been strategies to create a band gap in graphene by heteroatom doping or by surface modification. Nitrogen-doped graphene shows good electron mobility with n-type semiconducting behaviour, whereas boron-doped graphene is ambipolar [3]. Borocarbonitrides (BCNs) containing hexagonal BN and graphene domains of varying proportions have shown interesting electronic and gas adsorption properties [4]. TMDs include materials with a variety of properties like insulating HfS_2, semiconducting MoS_2 and metallic TaS_2 and $NbSe_2$. TMDs exhibit exotic features and with new properties arising from the valley polarization arising due to spin–orbit splitting [5]. In addition to the physiochemical properties, the layered materials have efficiently been used as materials in transistors, catalysts in water oxidation as well as reduction and oxygen reduction, supercapacitors and batteries [1]. It is noteworthy that cross-linked heterostructure of these 2D materials have shown interesting electrochemical and surface properties [6]. Stacking these 2D materials layer-by-layer increases not only the surface area but also the pore volume, which in turn enhances the gas sequestering properties. These newly designed cross-linked composites find applications in photochemical hydrogen evolution and supercapacitor applications. A schematic representation of the cross-linked 2D heterostructure is shown in scheme 1. In this article, we briefly describe the synthesis methods of the 2D materials and discuss the applications of graphene, TMDs and BCNs particularly in energy devices.

2. Synthesis

Synthesis of 2D nanosheets using micromechanical exfoliation of bulk single crystal by scotch tape gives high-quality single-layer as well as few-layer samples, which are ideal for studying various condensed matter phenomena. However, the yields are poor and therefore to study their properties the liquid or thermal exfoliation methods are being used widely [7]. Novoselov *et al* [8] first demonstrated the micromechanical cleavage of graphite crystal by scotch tape method to synthesize single-layer graphene. Chemical vapour deposition (CVD) on different metal surfaces yields single-layer to few-layer graphene with different carbon sources (methane, ethylene and acetylene) [9]. Subrahmanyam *et al* [10] produced good quantities of high-quality few-layer graphene (2–4 layers) using arc discharge of graphite in the presence of hydrogen atmosphere. Panchakarla *et al* [11] synthesized nitrogen-doped few-layer graphene by the arc-discharge method in the presence of ammonia or pyridine vapours to obtain 1–1.4 at% of nitrogen content, whereas under CVD conditions Wei *et al* [12] obtained ∼9 wt%. Li *et al* [13] thermally treated graphene oxide (GO) in the presence of ammonia at different temperatures (300–1100°C) to obtain 5 wt% of nitrogen content. Boron-doped graphene synthesized under similar conditions by the arc-discharge method

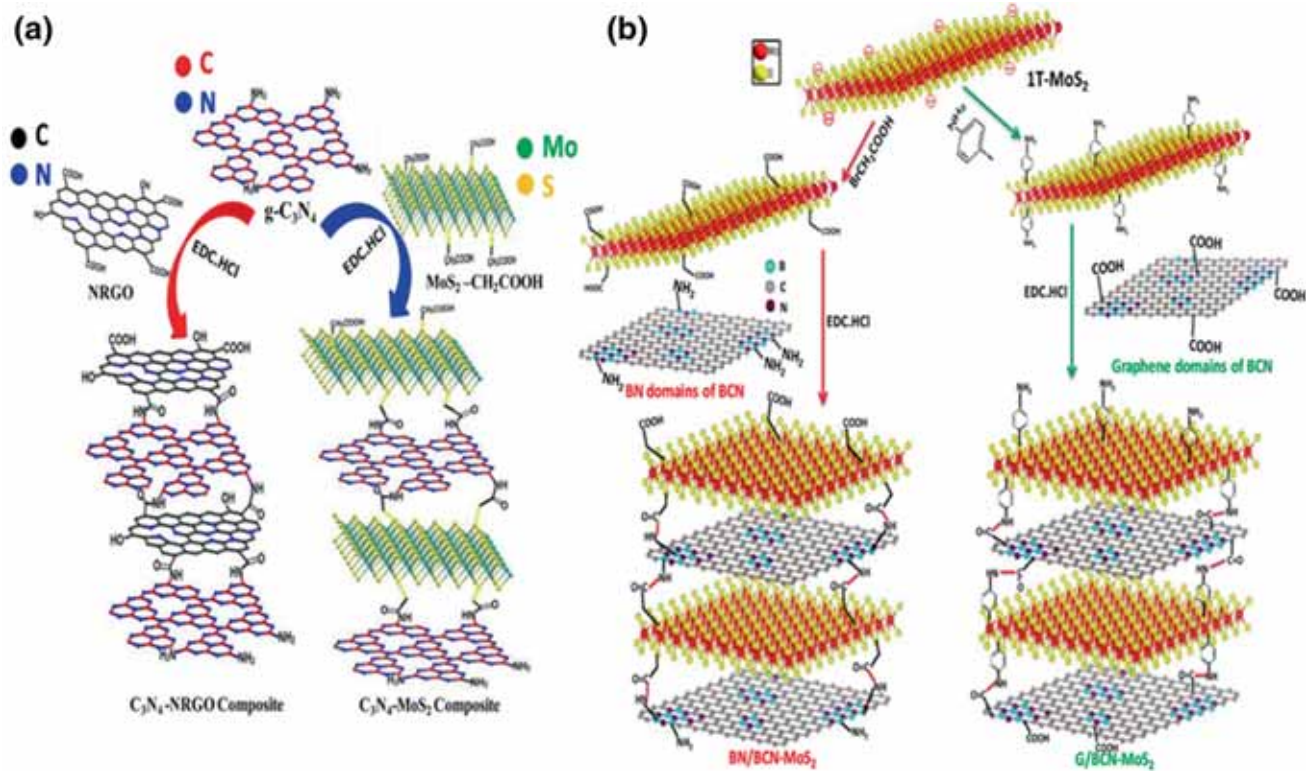

Scheme 1. Synthesis strategies for covalently bonded cross-linked (**a**) C_3N_4-NRGO and $C_3N_4-MoS_2$ composites and (**b**) cross-linked BN/BCN$-MoS_2$ and G/BCN$-MoS_2$ nanocomposites (EDC = 1-ethyl-3-(3-dimethylaminopropyl)carbodiimide). Adapted from refs [6,26]. Copyright 2016 Royal Society of Chemistry. Copyright 2017 American Chemical Society.

yields 1–3 at% of boron content in the presence of diborane [11]. BCNs, which contain both graphene and boron nitride domains, can be synthesized by heating activated charcoal, urea and boric acid at 900°C in an inert atmosphere [14]. The composition of BCN can be tuned by varying the contents of urea and boric acid.

Direct sonication in solvents like N-methyl-2-pyrrolidone can exfoliate single or few layers of 2D TMDs like MoS_2, $MoSe_2$, WS_2 and TaS_2 (figure 1a) [15,16]. The dispersing medium should have surface energies comparable to those of the materials to overcome the cohesive energy between the layers [15]. Chemical exfoliation of the 3D-bulk crystal can be used for mass production (∼100%) of exfoliated TMD nanosheets as exemplified by the use of n-butyl lithium dissolved in hexane as the intercalation agent (figure 1b) [17]. Interestingly, the semiconducting 2H-form of MoS_2 gets converted to the metallic 1T-MoS_2 after Li-intercalation and exfoliation [18], but the 1T-phase is not stable and reverts back to the 2H-form.

Large area films of few-layer 2D TMDs have been grown by physical vapour deposition or CVD under suitable conditions. Vapour-phase transport recrystallization from powders, thermal decomposition of thio salts or vapour-phase deposition methods that include sulphurization or selenization of metals or metal oxides yield high-quality TMDs [19–22]. Physical and chemical properties and the compositions of the products are controlled by adjusting the ratio of precursors as well as reaction conditions (figure 1c) [19]. Various physicochemical properties of the solvents such as polarity, viscosity and softness can affect the solubility and transport behaviour of the precursors during the synthesis process [23]. Mahler *et al* [24] have synthesized 1T-WS_2 and 2H-WS_2 nanosheets in a mixture of oleylamine, WCl_6, oleic acid and CS_2 by solvothermal method (figure 1d). The most important aspect of the solvothermal method is that it prevents the TMDs from oxidizing. Thus, the moderate temperatures together with the advantage of fast reaction kinetics and short processing time render it as a promising route to prepare homogeneous products on a large scale.

Cross-linked heterostructures (BCN-MoS_2 [25], MoS_2–nitrogen-doped graphene [26]) can be synthesized using a coupling reagent like N-(3-(dimethylamino)propyl) N′-ethylcarbodiimide hydrochloride (EDC·HCl) (scheme 1). With this strategy, any two layered structures can be cross-linked with suitable reagents [6]. C_3N_4 can be linked to both MoS_2 and graphene by EDC coupling. BCNs and functionalized graphene can be linked to MoS_2 and other layered structures. The cross-linking strategy offers versatility in linking two different layered materials, providing layer-by-layer stacking and new properties.

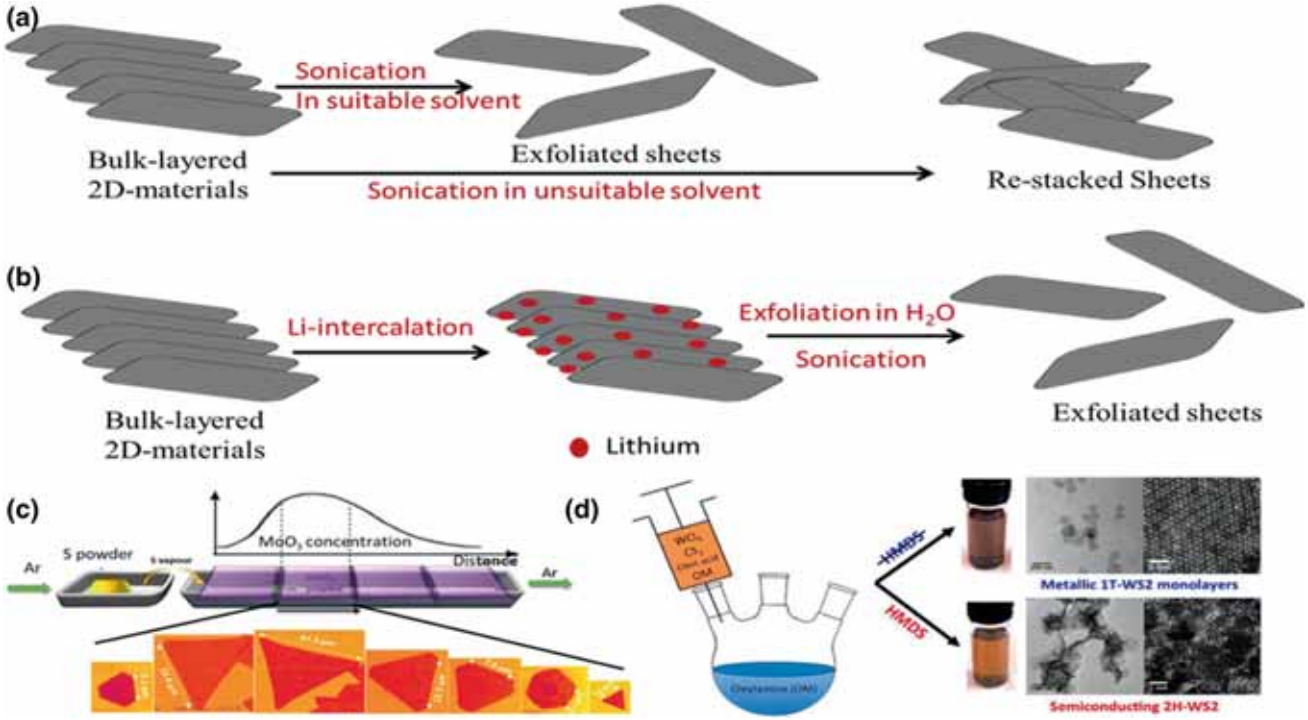

Figure 1. **(a)** Exfoliation of bulk 2D-layered materials either by probe or bath sonication in a suitable solvent can give high-quality single- to few-layer sheets. In unsuitable solvents the exfoliated sheets can be restacked. **(b)** Chemical exfoliation by Li-intercalation followed by exfoliation in water gives large-scale exfoliated single- to few-layer sheets. **(c)** Large-area sheets of 2D TMDs under suitable conditions can be synthesized. A schematic of synthesis of MoS_2 nanoflakes with different shapes. The concentration of MoS_2 is the determining factor in the evolution of these shapes during synthesis. The Ar flow rate is 100 sccm and reaction occurs on 300 nm SiO_2 coated Si-chip. Adapted with permission from ref. [19]. **(d)** Schematic of synthesis of 1T and 2H-WS_2. The crystal structure is different when HDMS is added, which shows the determining effect of the solvent. With suitable reaction conditions we can synthesize 2D materials from their precursors. Adapted from ref. [24]. Copyright 2014 American Chemical Society.

3. Transistors

Graphene is the most widely studied 2D material for transistor properties because of its extraordinary mobility of $\sim$25000 cm^2 V^{-1} s^{-1} at room temperature [27]. However, it is not possible to switch off the FET because of its delocalized electrons, hence showing poor on–off ratios (<10). Graphene nanoribbons with a small band gap (140 meV) show a conventional band transport at room temperature [28]. Optimization of graphene nanoribbons can give rise to useful FET properties. Reduced graphene oxide (RGO) has been used as a transistor, but the performance is less as compared with mechanically exfoliated graphene [29]. Fiori *et al* [30] have simulated carbon-dependent transfer characteristics in BCNs. The carbon-rich BCN showed high current transport, but poor on–off ratio, whereas the BN-rich BCN showed high on–off ratios. BCNs have mobility ranges from 6.4 to 10 cm^2 V^{-1} s^{-1} in FETs for carbon-rich samples [31]. Other 2D materials like TMDs, silicene and phosphorene have been recently studied [32]. The electronic mobility shows a relationship with the band gap and is shown for graphene, TMDs and other 2D materials and 3D materials in figure 2a [33].

TMDs possess diverse electronic properties from metal to insulator, with the band gap (1.1–2.2 eV) increasing with a decrease in the number of layers [34]. FETs based on mechanically exfoliated MoS_2 of thickness 8–40 nm with back-gated FET configuration have shown mobilities in the range of 0.1–10 cm^2 V^{-1} s^{-1} [8,35]. MoS_2 has gained attention over other TMDs because it is a robust, naturally abundant, high-quality crystal, which is readily mechanically exfoliated. Late *et al* [36] observed controllable hysteretic behaviour in atomically thin MoS_2 FET induced by adsorbed water molecules on MoS_2 surface and it can find potential applications in non-volatile memory devices. The first top-gated transistor based on monolayer MoS_2 reported by Radisavljevic [37] exhibited an on–off ratio of 10^8 with n-type conductivity and mobility of >200 cm^2 V^{-1} s^{-1} at room temperature (figure 2b). The high-k dielectric HfO_2 benefits the mobility of monolayer of MoS_2 [38–40], while the top gate geometry can allow a reduction in the voltage necessary to switch the device, which allows integration of multiple devices on a single substrate. Theoretically, a top-gated MoS_2 transistor with gate lengths of 15 nm can operate in a ballistic regime with on-current as high as 1.6 mA μm^{-1} and threshold current on–off ratio of

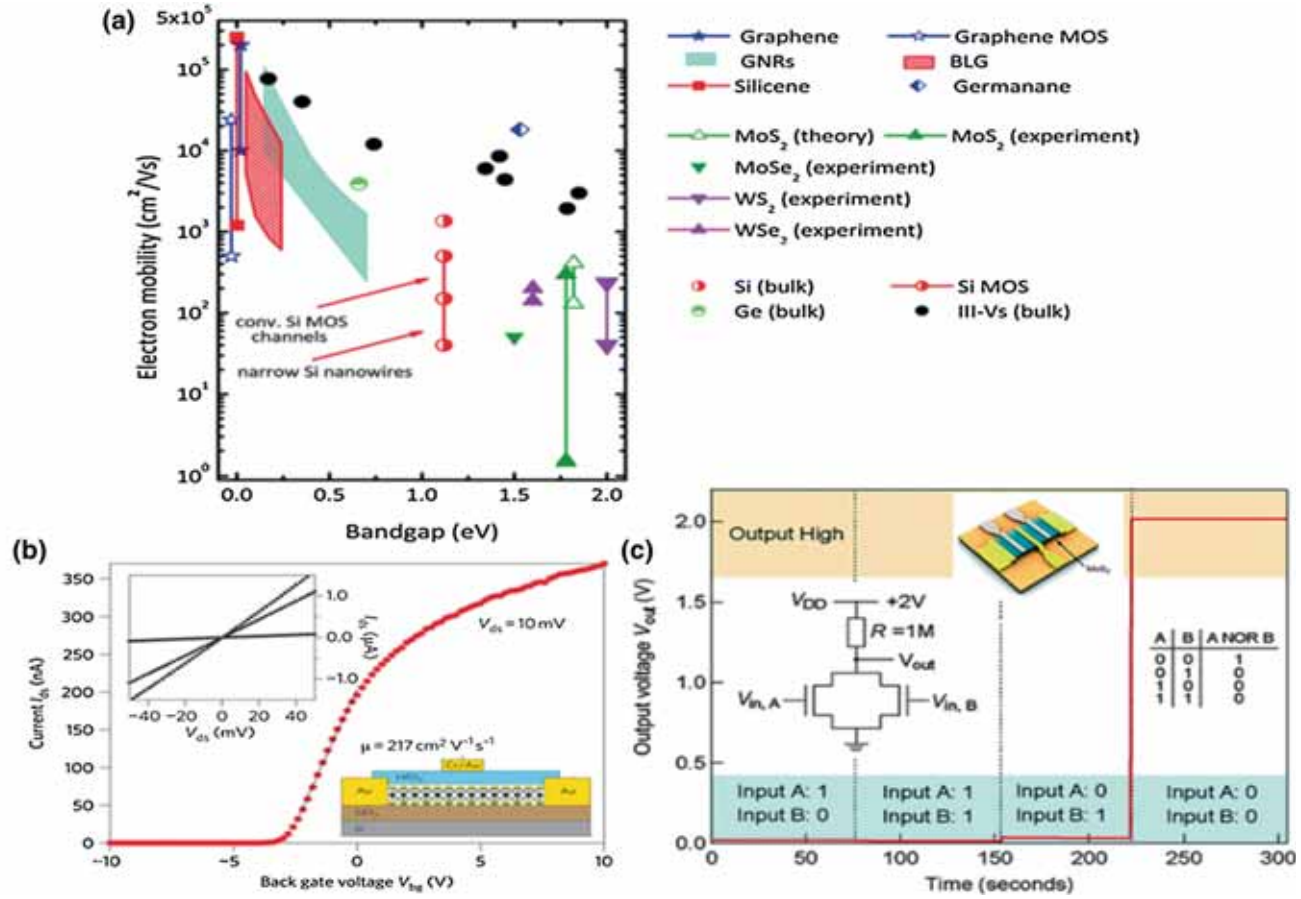

Figure 2. **(a)** Comparison of room-temperature electron mobility *vs.* band gap for different materials with 2D materials like graphene and TMDs. The figure was adapted with permission from ref. [33]. **(b)** Schematic of cross-sectional view of the top-gate FET of a monolayer MoS_2 (inset in right hand corner). Transfer characteristic for the FET with applied bias voltage V_{ds} (10 mV). The back-gate voltage (V_{bg}) is applied to the substrate while the top gate is disconnected. Drain–source current (I_{ds})–drain–source voltage (V_{ds}) curves acquired for V_{bg} at 0, 1 and 5 V. The figure is adapted from ref. [37]. **(c)** Schematic of a device for NOR gate based on single-layer MoS_2 (inset middle top). Two monolayer MoS_2 transistors are connected in parallel using an external 1 MΩ resistor as a load (left inset) the logic circuit is formed. The output voltage (V_{out}) is shown in various regimes for four different sets of input states (1,0), (1,1), (0,1) and (0,0) with response only, with both inputs in the low state. The truth table shows that these combinations can be shown as NOR gate operations (inset). Adapted from ref. [42]. Copyright 2016 Elsevier. Copyright 2011 Springer Nature. Copyright 2011 American Chemical Society.

10^{10} [41]. Radisavljevic *et al* [42] built a functional electronic circuit based on MoS_2 that is capable of performing digital logic operations (figure 2c). Ambipolar transport demonstrated in a thin (10 nm thick) MoS_2 electric double layer transistor using an ionic liquid as the gate to reach extremely high carrier concentrations of 10^{14} cm^2 with on–off ratio of 200 [43].

A promising approach is to stack different 2D-layered materials to make vertical heterostructures and hybrid devices with operating principles that are unlike those of conventional devices. Recently, FET with high switching ratio was achieved using two independently controlled graphene layers are separated by thin MoS_2 or h-BN layers, which act as tunneling barriers [44]. Similar heterojunctions with MoS_2 and highly doped germanium have been reported to exhibit low currents at a supply voltage <100 mV [45]. The implantation of 2D materials in electronic devices is still at research level, and some basic techniques are under development. The challenge is to increase the current density and reduce the contact resistance at least on the order of $<100\ \Omega$, especially for short channel length. A heterostructure design with doping or controlled growth can result in thinnest possible FETs with several opportunities in 2D-crystal electronics.

4. Sensors

4.1 *Gas sensors*

2D-layered materials, like graphene, are promising sensing materials due to their high surface area and low-single to noise ratio compared with 1D or 0D structures [46,47]. Graphene has substantial conductivity and exhibits changes

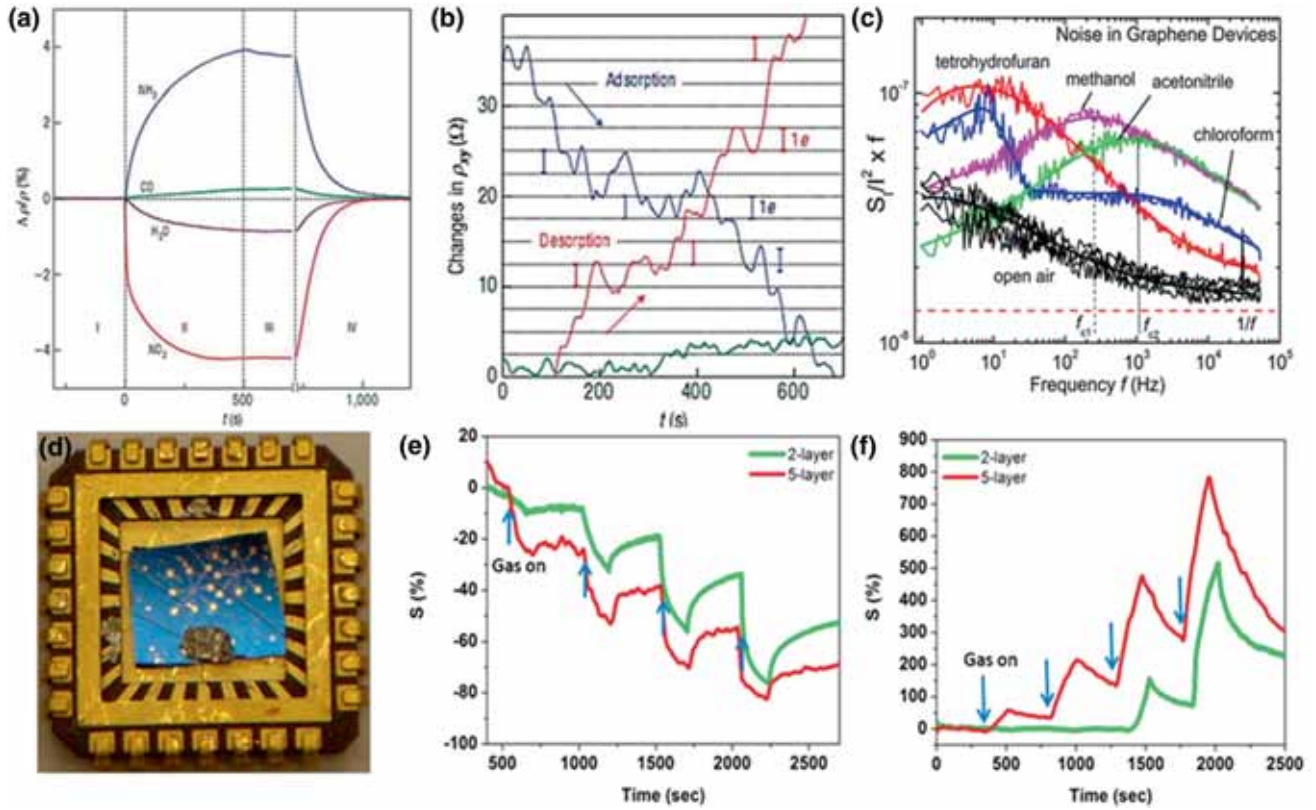

Figure 3. **(a)** The graph represents change in resistivity with respect to time over different stages of gas sensing procedure of various gases (1 ppm). Vacuum (Region I), when gas in introduced (Region II) on exposure to gas, evacuation of the experimental set-up (Region III) and annealing at 150°C to de-adsorb gas (Region IV). The positive sign indicates electron doping while the negative sign indicates hole doping. **(b)** The change of Hall resistivity ρ_{xy} observed near the neutrality point through adsorption (blue curve) and desorption (red curve) of diluted NO_2. Green curve is when the sensor is exposed to pure He, which is used as a reference. Adapted from ref. [49]. **(c)** Analysis of product of noise spectral density (SI/I_2) multiplied by frequency (f) *vs.* f for the sensor upon exposure to different vapour samples along with open air. Adapted from ref. [52]. **(d)** Photograph of the transistor-based MoS_2-sensing device mounted on the chip. Sensing behaviour of **(e)** NH_3 and **(f)** NO_2 gas with and without applying back-gate voltage ($V_g = 15$ V) for two-layer MoS_2 (arrows indicate concentration of gases at 100, 200, 500 and 1000 ppm of each gas). Adapted from ref. [64]. Copyright 2017 Springer Nature. Copyright 2017 American Chemical Society.

in conductivity on interaction with foreign molecules. For instance, H_2O molecule does not induce much change in the localized impurity states in graphene but alters the conductivity noticeably (figure 3a) [48]. An electron-donating molecule such as NH_3 decreases the concentration of carriers while NO_2, an electron-withdrawing molecule, increases the concentration of carriers (figure 3a). Similarly, halogen molecules or alkali elements act as dopants and contribute electron or hole doping. A single-layer graphene-based gas sensor synthesized by Schedin *et al* [49] has a detection limit of ppb for NO_2 molecule, which was further improved using Hall geometry (figure 3b). Since then, single-layer graphene has been an attractive material to detect gases or small organic molecules like methanol, THF, acetonitrile and chloroform [50,51]. Interestingly, vapours of different molecules induce noise with a different frequency, which distinguishes the signal to detect them both qualitatively and quantitatively (figure 3c) [52]. A drawback of pristine graphene is that it is highly sensitive to contaminants which can be overcome with illumination with UV light as exhibited by Chen *et al* [53]. The sensor was highly sensitive to N_2O, NH_3, SO_2 and H_2O under flowing N_2 carrier gas with detection limits in the range of 39–136 ppt.

Chemically exfoliated graphene, hydrogenated graphene and RGO show excellent sensing properties [47]. RGO has shown high sensitivity to H_2O and gases like NO_2 and Cl_2 at low concentrations [54,55], which was further increased by sulphonation [56]. Chemically reduced few-layer graphene efficiently detects DNA bases, nicotinamide adenine dinucleotide (NADH), neurotransmitters, oxidase/dehydrogenase-related molecules, other molecules like acetaminophen, uric acid or ascorbic acid and other biomolecules [57,58]. Electrochemical sensors based on RGO can detect biomolecules at minute concentrations through impedance spectroscopy [59,60]. BCN was earlier used as a sensor for real-time monitoring of slag oxidation by

measuring the partial pressure of oxygen [61]. Recently, BCN has shown sensor properties for uric acid and dopamine [62].

Like graphene, MoS_2 has shown remarkable sensors properties. FET devices of mechanically exfoliated MoS_2 have been used as NO sensors with a sensitivity of 300–800 ppb, depending on the number of layers [63]. Similar to graphene, acceptor molecule like NO_2 and electron donating molecule like NH_3 increases or decreases the resistance of MoS_2, respectively, based on charge transfer mechanism (figure 3d–f) [64]. Single-layer MoS_2 can detect DNA and other biomolecules by photoluminescence spectroscopy [65]. MoS_2 can distinguish between the single- or double-stranded DNA due to the difference in fluorescence-quenching ability [66]. DNA can also be detected with FET devices based on MoS_2 [67]. Graphene has generally better sensing ability. The sensing properties of the gases by graphene and other TMDs are listed in table 1.

4.2 *Photodetectors*

Single-layer graphene has optical absorption over a wide range as well as strong interband transitions and acts as an ultrafast photodetector [70,71]. Chemically reduced graphene offers cheaper, tuneable, scalable and solution-processed UV and IR detectors with good photoresponse and on–off ratio [72,73]. The detectors show a strong response to signals as weak as human-hand. However, for photodetector and photovoltaic applications, materials with suitable band gap is preferred.

MoS_2 possesses band gap with properties suitable for photodetector and photovoltaic applications. Single- and double-layer MoS_2 have been used as a detector of green light, while three-layer MoS_2 detects red light [74]. Chemically exfoliated MoS_2 was reported to show near-IR absorbance, where MoS_2 shows 7.8 times greater absorbance than that of RGO [75,76]. Phototransistors made using single-layer MoS_2 have shown fast response with a switching duration of 50 ms and good photosensitivity [77]. The responsivity of such devices can be tailored by the gate voltage, making them even better than graphene-based devices. Being a direct-band-gap semiconductor, single-layer MoS_2 phototransistors, with improved contacts and positioning techniques, show ∼106 times better responsivity than that of graphene [78]. Heterostructures of TMDs have shown strong sensing properties for both light and matter [79]. Photodetectivity of graphene and TMD-based devices is shown in table 2.

5. Supercapacitors

Supercapacitors are electrochemical energy storing devices that find applications because of their high energy and power density [86]. Carbon-based materials such as carbon nanotubes, carbon nanofibres and graphene have shown excellent supercapacitor properties due to their high surface area and electrical conductivity [87]. Vivekchand *et al* [88] reported the first graphene-based supercapacitor, wherein few-layered graphene exhibits high specific capacitance up to 117 F g^{-1} in aqueous electrolytes and an energy density of 31.9 Wh kg^{-1} in an ionic liquid. Supercapacitors made of chemically modified graphene have shown a maximum specific capacitance of 135 F g^{-1} in aqueous electrolyte [89], while supercapacitors made of activated graphene with macro- and mesopores have shown a capacitance of 174 F g^{-1} in an organic electrolyte with an energy density and power density of 74 Wh kg^{-1} and 338 kW kg^{-1}, respectively [90]. The surface area of graphene has been increased up to 2400 m^2 g^{-1} by microwave exfoliation or by KOH activation of GO. Such

Table 1. The sensing properties of graphene and TMDs.

Sensor material	Target gas	Sensitivity and limit of detection	References
Graphene			
Mechanically exfoliated graphene	NO_2	$\Delta R > 2.5\,\Omega$ for one electron; single-molecule detection	[49]
Mechanically exfoliated graphene	CH_3OH, C_2H_5OH, THF, CH_3CN	Using frequency *vs.* resistivity pattern variation of each vapour molecule	[52]
CVD-grown graphene	NO_2, O_2, SO_2, NO	$\Delta R = 0.2$–0.5% ppm^{-1}; 158 ppq–103 ppt	[53]
RGO (printable sensor)	NO_2, Cl_2	500 ppb–100 ppm	[68]
Sulphonated/ethylenediamine-modified RGO	NO_2	$\Delta G/G = 0.443$ ppm^{-1} 3.6 ppm	[56]
MoS_2			
Mechanically exfoliated 1L-MoS_2	Selective detection of electron donors like triethylamine, selectivity better than that of CNT	10 ppb	[69]
Mechanically exfoliated 2&5L-MoS_2	NO_2, NH_3, relative humidity	1.37% ppm^{-1}	[64]

Table 2. Photo-detection activities of graphene and 2D-TMDs.

Device type	Responsivity	Quantum efficiency (%)	References
Graphene			
Photoconduction	∼0.1 mA W^{-1}	—	[80]
Heterojunction	100 mA W^{-1}	—	[81]
Bolometric	0.2 mA W^{-1}	10–30%	[82]
TMDs			
In-plane			
Photoconduction	880 A W^{-1}	—	[78]
Heterojunction	210 mA W^{-1}	∼30%	[83]
Out-of-plane			
Photoconduction	100 mA W^{-1}	0.2%	[84]
Heterojunction	∼100 mA W^{-1}	∼10–30%	[85]

high-surface-area graphene shows a specific capacitance of 166 F g^{-1} [91] and 191 F g^{-1} [92]. In-plane fabricated few-layered RGO supercapacitor electrode shows a capacitance of 394 μF cm^{-1} in PVA−H_3PO_4 solid-state electrolyte [93]. The performance of graphene clearly depends upon the number of layers, surface area and pore structure [88,91]. The intrinsic capacitance of graphene can be increased by doping with hetero-atoms such as nitrogen and boron, which in turn tune the electronic properties [3].

Nitrogen-plasma-processed graphene shows nearly four times higher capacitance (∼280 F g^{-1}) than that of unprocessed graphene with excellent cycling stability and power densities [94]. The study predicts that the nitrogen atoms present between edges and basal planes of graphene are the primary reason behind the increase in capacitance. Crumbled nitrogen-doped graphene synthesized by heating (750 or 900°C) GO in ammonia shows high capacitance (248 F g^{-1}) due to its high pore volume, nitrogen content and the wrinkles formed during the synthesis [95]. RGO treated with urea at different temperatures shows increase in specific capacitance due to the increase in nitrogen content [96]. Heavily nitrogenated graphene (NGO) synthesized by microwave method using urea as the nitrogen source shows extraordinary supercapacitor properties [97]. Figure 4a shows the cyclic voltammogram of heavily nitrogenized graphene. The cyclic voltammogram is quasi-rectangular, which confirms it to be an ideal capacitor with a specific capacitance of 461 F g^{-1}. The Nyquist plot shows little charge transfer resistance in these materials as shown in figure 4b. The stability of NGO is shown in figure 4b, where the material shows excellent cyclic stability with just 2.7% decrease from the initial specific capacitance as shown in figure 4c. The energy density and power density are 44.4 Wh kg^{-1} and 852 W kg^{-1}, respectively (figure 4d). The reason behind the increase in specific capacitance is the high nitrogen content of graphene. There are three different nitrogens present in the N-doped graphene, namely pyrrolic, pyridinic and graphitic nitrogen. Pyrrolic and pyridinic nitrogens are found to be electrochemically active and cause an increase in capacitance, whereas the graphitic nitrogen increases the conductivity of the material [98].

Boron-doped graphene also shows an increase in capacitance compared with pristine graphene. Boron-doped graphene synthesized by heating GO with boric oxide shows a capacitance of 172 F g^{-1} at 0.5 A g^{-1} with good stability over extended cycling [99]. The increase in capacitance is due to the formation of oxygen-containing functional groups such as BC_2O/BCO_2 while doping. Porous B-doped graphene made by Fried ice method exhibits a high surface area of 622 m^2 g^{-1} and a capacitance of around 281 F g^{-1} [100]. Borane-reduced GO shows a capacitance of 200 F g^{-1} with good stability over 4000 cycles [101]. Laser-patterned B-doped graphene micro-supercapacitor shows an excellent areal capacitance of 16.5 mF cm^{-2}, which is 3 times higher than that of pristine graphene devices [102]. Dielectric barrier discharge plasma-based boron-doped graphene exhibits a capacitance of 446 F g^{-1} at 0.5 A g^{-1} [103]. Sponge-like B-doped graphene nanosheets synthesized hydrothermally using boric acid shows a capacitance of 113 F g^{-1} at 1 A g^{-1} [104].

BCN synthesized by heating urea and boric acid with activated charcoal shows excellent supercapacitor properties [96]. In addition to capacitor properties, it also possesses high surface area and gas sequestering abilities [14]. $BC_{4.5}N$ has the highest specific capacitance of 178 and 240 F g^{-1} in an aqueous electrolyte and in an ionic liquid, respectively. BCNs prepared from exfoliated graphene show capacitance in the 276–306 F g^{-1} range [31,105].

Layered TMDs such as MoS_2 and WS_2 are being explored in the area for supercapacitor applications [1]. Thus, chemically exfoliated 1T MoS_2 nanosheets exhibit capacitance values ranging from 400 to 700 F cm^{-3} in aqueous electrolytes and the material can be charged up to a high voltage (3.5 V) of organic electrolytes [106]. Porous MoS_2 nanosheets exhibit a capacitance of 330 mF cm^{-3} with high power density and cyclic stability [107]. Laser-patterned MoS_2 nanofilms exhibit a volumetric capacitance of 178 F cm^{-3}, which is better than that of some of the graphene-based

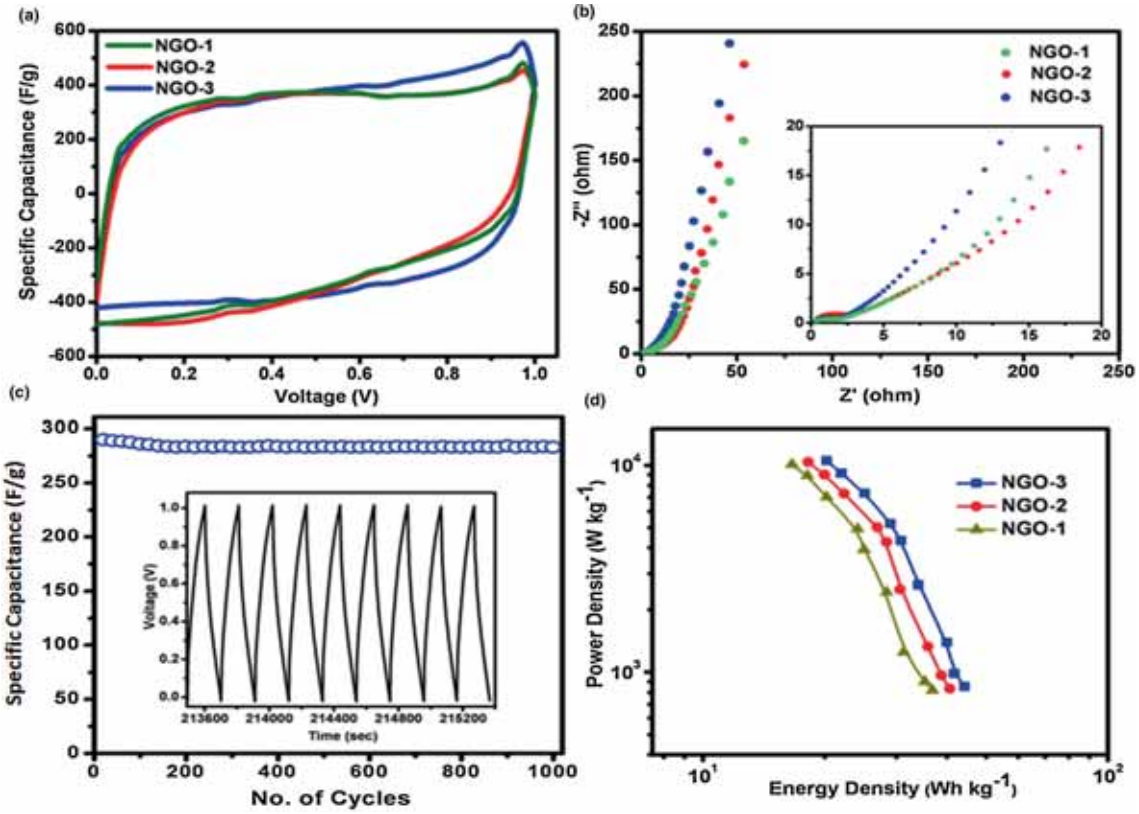

Figure 4. **(a)** Cyclic voltammograms of NGOs at a scan rate of 20 mV s^{-1}. **(b)** Nyquist curves for NGO electrodes. **(c)** Cyclic stability of NGOs (the inset shows the charge–discharge curves of the last few cycles). **(d)** Ragone plots of NGO-based supercapacitors. Adapted from ref. [97]. Copyright 2013 Royal Society of Chemistry.

devices [108]. The capacitance of MoS_2 can be tuned by making composites with graphene, where the MoS_2–graphene composites have shown extraordinary supercapacitor properties [109–111].

6. Oxygen reduction reaction

The oxygen reduction reaction (ORR) plays an important role in fuel cell technology and the reaction kinetics are generally sluggish. The most used catalyst is Pt, which is expensive and less abundant. 2D materials like graphene and transition metal chalcogenides have shown good prospects as ORR catalysts [1]. Nitrogen-doped graphene shows phenomenal ORR activity with an electron transfer of 4. Nitrogen-doped graphene synthesized by CVD shows excellent ORR activity in alkaline medium with good stability and overpotential [112,113]. Qu *et al* [112] have shown that N-doped graphene is resistant towards carbon monoxide poisoning when compared with platinum in alkaline medium. Rotating ring–disk electrode (RRDE) voltammograms of the N-graphene film are shown in figure 5a. Nitrogen-doped graphene shows almost 3 times higher current density compared with that of platinum with an electron transfer ranging from 3.6 to 4. Electrocatalytic oxidation of methanol is shown in figure 5b, with N-graphene showing excellent stability. Pt–C electrode gets poisoned under carbon monoxide (CO), whereas N-graphene electrode is unresponsive under the same conditions as shown in figure 5c. N-graphene electrode shows excellent stability towards ORR even after 200000 continuous cycles (figure 5d). N-doped graphene prepared by pyrolysis of polyaniline with graphene shows good ORR activity with large kinetic-current density [114]. N-doped graphene synthesized by ball milling [115], pyrolysis of GO–melamine and GO–dicyandiamide [116] and microwave [97] are also reported to exhibit good electrocatalytic activity comparable to that of platinum. Theoretical calculations predict that nitrogen doping in graphene introduces asymmetry spin density and atomic charge density, which in turn enhances the electrocatalytic activity [117].

High-surface-area BCNs with different proportions of nitrogen and boron show excellent ORR activity with an electron transfer of 4 in alkaline medium [118], whereas, BCNs made with thermal annealing of GO with boric acid and ammonia have shown good ORR activity and methanol tolerance better than that of platinum [119]. BCNs made from exfoliated graphene have shown similar electrocatalytic activity [31,105]. It is to be noted that boron-doped [120] and B,N-doped graphene [121] are also reported to show good ORR activity.

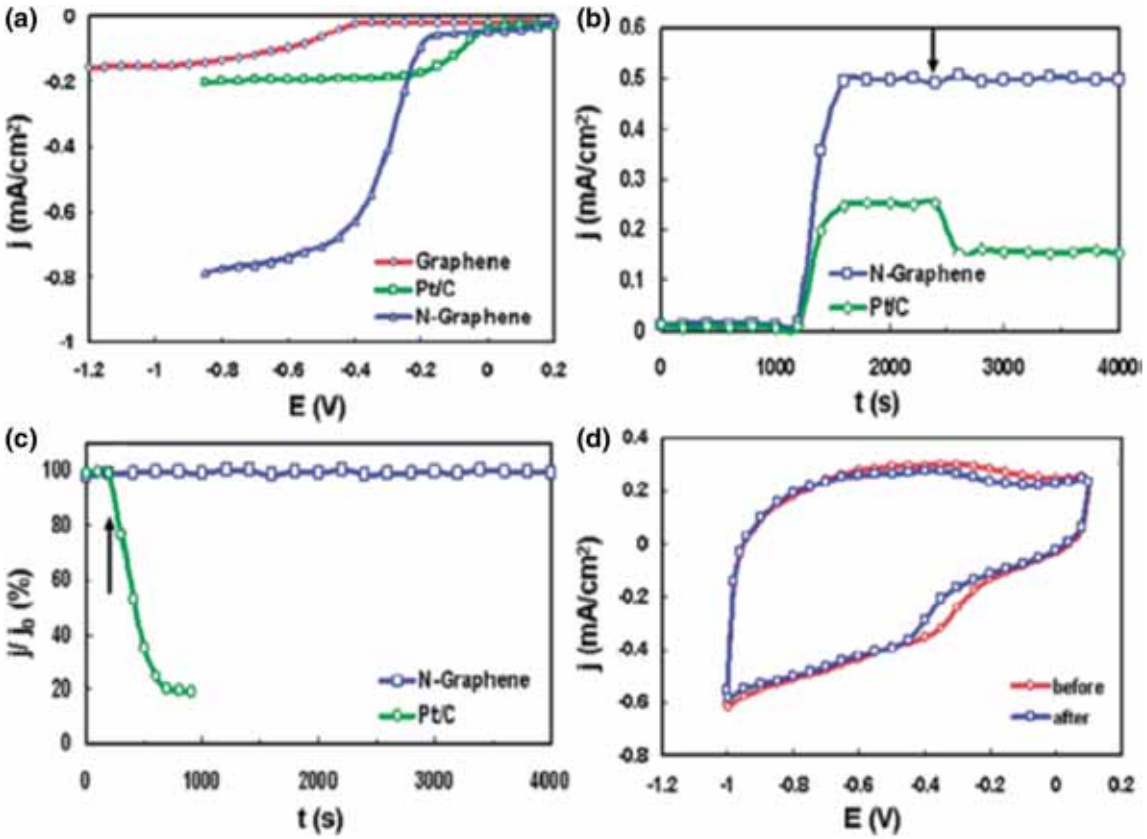

Figure 5. **(a)** RRDE voltammograms for the ORR in air-saturated 0.1 M KOH. **(b)** Current density (j)–time (t) chronoamperometric responses obtained at the Pt–C. **(c)** Current (j)–time (t) chronoamperometric response of Pt–C and N-graphene electrodes to CO. **(d)** Cyclic voltammograms of N-graphene electrode a continuous potentiodynamic swept for 200000 cycles. Adapted from ref. [112]. Copyright 2010 American Chemical Society.

MoS_2 particles show improved ORR catalytic activity compared with bulk MoS_2 [122]. The size and the exposed Mo edges of the MoS_2 play a role in the enhanced activity. MoS_2–graphene nanocomposites have shown significant ORR activity compared with pristine MoS_2 [110]. MoS_2 composites with several carbon materials are also reported to exhibit better activity when compared with MoS_2 [123].

7. Lithium-ion batteries

Lithium-ion batteries are playing increasingly important role in electronic devices and in energy storage due to their high energy density and power density capabilities. 2D materials like graphene and MoS_2 show good charge storing ability because of the fast ion-conduction and reversible Li-intercalation and de-intercalation properties [5]. Nitrogen-doped graphene deposited on Cu foils have shown double reversible discharge capacity [124]. Thermally prepared nitrogen-doped graphene from GO and ammonia exhibits a reversible capacity of 684 mAh g^{-1}. Glucose-based synthesis of nitrogen-doped graphene with different nitrogen dopants enhanced the reversible capacity of 832.4 mAh g^{-1} with very good cycling stability [125]. BCNs prepared by high-temperature reaction of carbon, boric acid and urea have shown exceptional stability of more than 100 cycles and exhibit specific capacities ranging from 710 to 150 mAh g^{-1} [126].

Haering *et al* [127] reported the first MoS_2-based Li-batteries with a charge capacity of 750 mAh g^{-1} after 20 cycles at a current density of 50 mA g^{-1}. The charge capacity can be increased up to ~1000 mAh g^{-1} by making the MoS_2 nanosheets hydrothermally [128]. In addition to Li ion batteries, MoS_2 nanowalls grown on alumina substrates using atomic layer deposition exhibit exceptional sodium ion battery capabilities [129]. The nanowalls show a specific capacity value of 2726 and 2078 mAh g^{-1} in the 1st and 10th cycle, respectively (figure 6a). Stable capacity is observed in the voltage range of 1.2–3.0 V, yielding a reversible capacity of 980 and 590 mAh g^{-1} in 1st and 100th cycles, respectively (figure 6b and c). The capacities were stable even at high current densities (figure 6d). MoS_2–graphene improves the reversible capacity of 1290 mAh g^{-1} at a current density of 100 mA g^{-1} up to 50 cycles [130].

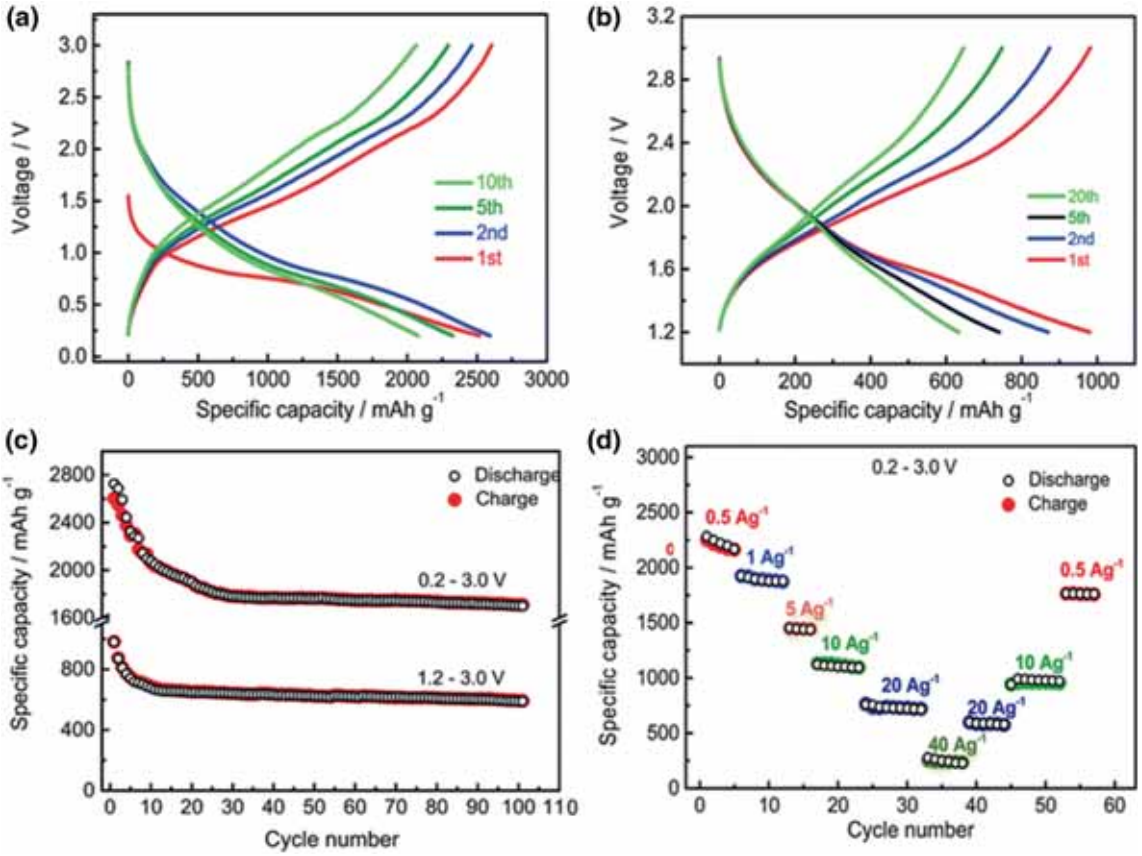

Figure 6. **(a, b)** Galvanostatic charge–discharge curves in different voltage ranges, **(c)** cycling stability at 0.5 A g^{-1} and **(d)** rate capability of ALD-grown MoS_2 *vs.* Li for 0.2–3.0 V. Adapted from ref. [129]. Copyright 2018 Royal Society of Chemistry.

8. Hydrogen evolution reaction

Hydrogen evolution reaction (HER) refers to splitting water into hydrogen usually in the presence of sacrificial reagents to enhance the reaction by overcoming the slow water oxidation by a facile one. HER can be achieved either by electrochemical, photochemical or photo-electrochemical means and photochemical method is being used preferably. In electrochemical HER, a catalyst with thermo-neutral onset potential ($\Delta G \sim 0$) catalyst like Pt is being used. However, the scalability is limited due to the exorbitant cost of Pt. Two-dimensional TMDs have shown promising HER activity with near-thermoneutral onset potential. Moreover, these materials offer strong structure and activity relationship, which offers tremendous scope to improve the activity of these catalysts through various strategies.

Graphene-based catalysts are stable and durable with good electrical and thermal properties beneficial for the conduction of heat generated during reactions, the good electric conductivity rendering the materials candidates as electrocatalysts and as supports. Introduction of edges, defects, dislocations or doping with non-metals favours the catalytic reactions [131]. Functionalizing with oxygen, hydrogen or halogens can also alter the electronic properties of graphene. BCNs, especially BC_7N, have shown high potential to replace Pt, in terms of low onset-potential, high current density along with commercial scalability as they are a non-metal catalyst [132]. GO possesses a band gap that depends on the degree of functionalization and exhibits HER in pure water and in aqueous methanol solution on irradiation [133], which is further enhanced by loading Ni or NiO [134]. However, GO is primarily used with direct-band-gap semiconductors like TiO_2, CdS or dye (Eosin Y) as an electron transport bridge or redox mediator due to its high electronic conductivity for HER [135].

Recently, MoS_2 nanostructures have received considerable attention for HER. The edge sites can be increased by vertically growing MoS_2 or forming inorganic fullerenes (IFs). Nanostructuring can increase the number of active sites and thereby increase current density. Seo *et al* [136] find that increasing the interlayer spacing between MoS_2 layers increases the HER activity of MoS_2 colloids significantly (figure 7a). The increased inter-layer spacing allows easy access of water molecules to HER site. The basal planes can

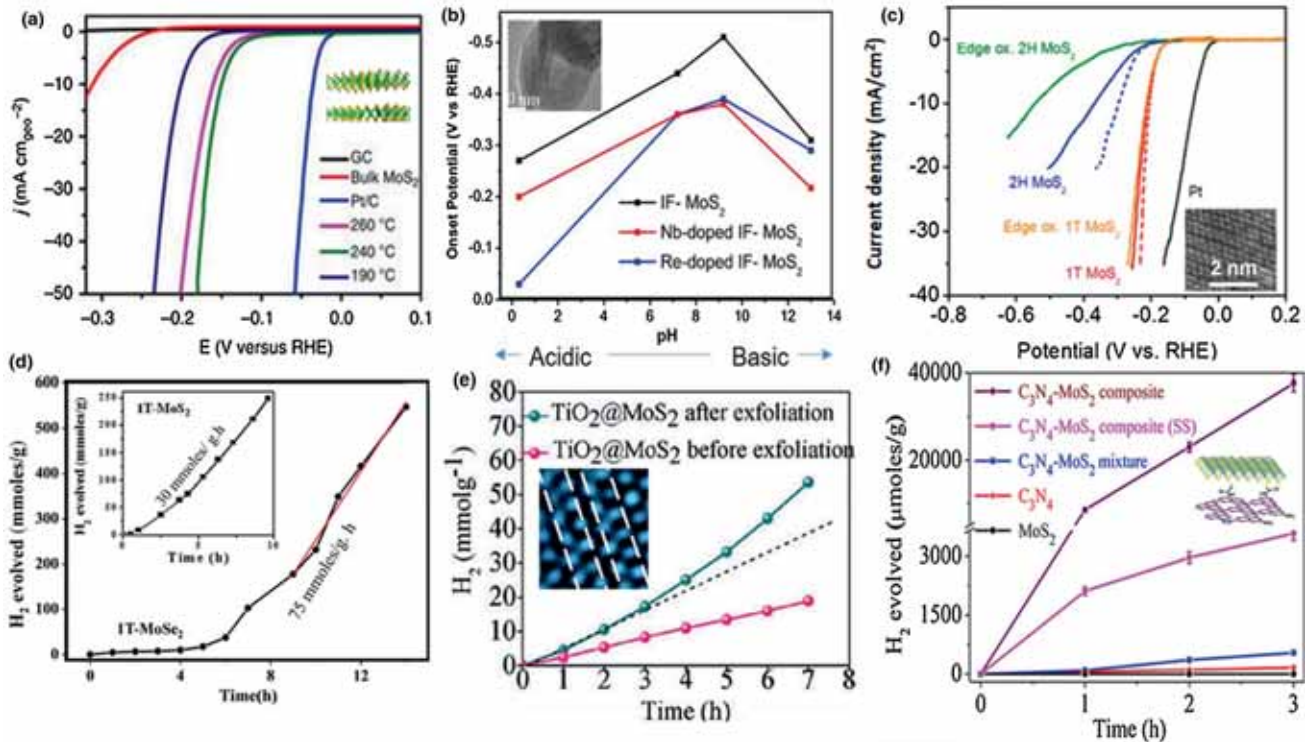

Figure 7. **(a)** Nanostructuring of MoS_2 increases the interlayer spacing between the layers, allowing water molecules, along with creation of edge sites; edge sites along with defect sites increase the HER activity of the catalyst. The activity of nanostructured MoS_2 is higher than that of bulk MoS_2. Adapted from ref. [136]. **(b)** Doped-inorganic fullerene (IF)–MoS_2 (inset) integrates the idea of activating basal planes by doping in addition to maximizing edge sites by morphology change. The doped sample is stable and works at all pH levels. Adapted from ref. [138]. **(c)** The phase-engineered 1T-form of MoS_2 shows high current density compared with 2H-MoS_2, which is attributed to current-active basal planes. The oxidized edge sites of 1T-form show high HER activity, which implies that the basal plane is also active unlike in 2H-form. Adapted from ref. [139]. **(d)** Similarly, 1T-form of MoS_2 and $MoSe_2$ shows high HER activity in Eosin Y (EY) dye-sensitized in triethanolamine solution. Adapted from ref. [142]. **(e)** 1T-MoS_2 was stabilized on TiO_2, which showed stability for a year (inset image). The 1T-form is self-stabilized during HER evolution in dye-based HER. Adapted from ref. [143]. **(f)** The covalently linked $C_3N_4-MoS_2$ is highly active as compared with its individual components or physical mixture. The covalently linked sample has greater charge transfer as compared with physical mixture. Adapted from ref. [26]. Copyright 2013, 2015 and 2017 American Chemical Society. Copyright 2013 and 2016 John Wiley and Sons Ltd. Copyright 2014 AIP Publishing.

be activated either by creating a vacancy, phase-engineering, doping or substitution with other transition metals (Nb, Re) or non-metals (Se, Cl or P) [137]. Chhetri *et al* [138] have integrated two strategies simultaneously by the modifying electronic structure coupled with increased edge sites in a doped IF of MoS_2. Re- and Nb-doped in IF-MoS_2 with lower onset potential exhibit increased HER activity. The catalysts perform at all pH values (0–14) and even in sea-water (figure 7b) [138]. Another strategy to activate both basal planes and edge sites is by phase engineering, by transforming the stable 2H-MoS_2 to metallic-1T-MoS_2, which activates the basal planes along with increasing the overall conductivity of the film [139]. The edge sites of 1T-form did not show any decrease in activity, whereas the oxidized edge-site 2H-MoS_2 have shown a considerable decrease in activity. The study signifies the importance of active basal planes in 1T-form for its enhanced activity (figure 7c). Covalently linked MoS_2 with BCN have shown high activity with a low-onset potential close to Pt [25]. Hybrid composites of TMDs with other materials such as carbonaceous materials or metals can enhance the efficiency synergistically [140].

In photochemical HER, MoS_2 has shown immense potential as the catalyst owing to its suitable band position. However, due to indirect band gap, it needs an external light-harvesting system like a dye or semiconductor to harvest its full potential [137]. 2H-MoS_2 has poor catalytic HER performance and needs to be modified. Rao and co-workers have demonstrated superior catalytic activity of the metallic 1T-phase over that of the semiconducting 2H-phase in $MoSe_2$ and MoS_2. In the Eosin Y(EY)–triethanolamine (TEOA) based photosystem, 1T-phase exhibits an activity 600 and 900 times superior to that of 2H-phase for MoS_2 and MoS_2, respectively. As the HER activity of the basal planes is similar to that of edge sites, 1T-phase has superior activity. The strategy captures the idea of nanostructuring, activating

Table 3. Summary and role of graphene or MoS_2 in photocatalytic hydrogen generation system.

Photocatalyst system	Reaction conditions	Activity (mmol h^{-1} g^{-1})	Role of graphene or TMDs	References
Graphene-based catalyst				
P25–RGO	Methanol; 300 W Xenon lamp	0.74	Charge mediator	[144]
CdS–RGO [Pt]	Lactic acid	56	Charge mediator; Pt acts as HER site	[145]
Eosin Y (EY)–RGO [Pt]	Triethanolamine (TEOA); 300 W Xenon lamp	4.71	Charge mediator; Pt acts as HER site	[146]
Graphene oxide	Methanol; 300 W Xenon lamp	5.6	HER site; highly functionalized	[134]
MoS_2				
EY–MoS_2	TEOA; 300 W Xenon lamp ($\lambda \geq 420$ nm)	0.05	Acts as a HER site	[141]
EY–1T-MoS_2	TEOA; 100 W halogen lamp	30.00	Activates basal plane along with edge sites for HER	[141]
EY−1T-$MoSe_2$	TEOA; 100 W halogen lamp	75.00		[142]
EY−RGO−MoS_2	TEOA; 100 W halogen lamp	3.30		[141]
EY–NGO−MoS_2	TEOA; 100 W halogen lamp	10.5	N-doping improves charge conductivity of GO–MoS_2 composite	[141]
	TEOA; 400 W Xenon lamp ($\lambda \geq 400$ nm)	42.0		
EY−BCN−MoS_2	TEOA; 100 W halogen lamp	7.0	Covalent-linking across the network increases the efficient charge transfer	[25]
CdS−MoS_2	Na_2S, Na_2SO_3; 300 W Xenon lamp ($\lambda \geq 420$ nm)	5.40	HER site; increases charge separation efficiency across CdS–MoS_2 heterojunction	[147]
g-C_3N_4−MoS_2 covalently linked	TEOA; 400 W Xenon lamp ($\lambda \geq 420$ nm)	12.78	HER site; directional nano-heterojunction increases efficient charge transfer along with heterojunction	[26]
EY−TiO_2−MoS_2	TEOA; 300 W Xenon lamp ($\lambda \geq 420$ nm)	16.70	HER site; increases charge separation efficiency	[143]
CdS–graphene–MoS_2	Na_2S, Na_2SO_3; 300 W Xenon lamp ($\lambda \geq 420$ nm)	9.00	HER site; charge efficiency increases in hybrid co-catalyst	[148]

basal planes coupled with increased metallicity for better charge transport in and between the layers (figure 7d) [141,142]. However, the 1T-phase is less stable, and therefore the remarkable HER activity cannot be entirely harvested. Duan and co-workers have grown TiO_2 nanotubes and grafted 1T-MoS_2 on its surface using an Eosin Y dye-sensitized system where the 1T-MoS_2 phase stabilizes itself during the process of hydrogen evolution and it is stable even after one year. The adsorption on H-atoms along with the catalyst support stabilizes the phase, which can provide robust, high-performing catalyst for long-term use (figure 7e) [143]. Covalently linking 2H-MoS_2 to other 2D materials like BCN and C_3N_4 is a way to solve most of the problems by integrating multiple problems [25,26]. The layer-by-layer directional linking of C_3N_4 with MoS_2 increases the activity of C_3N_4 by 246 fold. The enhanced activity is attributed to charge transfer across the network through space and bonds because of the direct overlapping of the layers and short conducting bonds (figure 7f) [26]. Table 3 summarizes the role of graphene and TMDs in photocatalytic hydrogen generation.

9. Mechanical properties

Graphene possesses unique mechanical properties with an elastic modulus of ~1 TPa and a theoretical strength of ~130 GPa. Graphene can be used as a reinforcement in polymer matrix such as poly(methyl methacrylate) (PMMA) or polyvinyl alcohol (PVA). The mechanical properties of graphene (0.6 wt%)-reinforced PVA and PMMA–matrix composites show an increase in both the elastic modulus (3.65 GPa) and hardness (153 MPa) [149]. The mechanical properties of the graphene–polymer matrix were further improved by adding single-walled carbon nanotubes [150]. Figure 8 shows the variation of the nanohardness (H) *vs.* elastic modulus (E) as a function of the nanocarbon content. The synergy between the two nanocarbons increases the mechanical properties up to 400%. Graphene-like boron nitride has shown improved mechanical properties depending upon the number of layers. When three BN layers are incorporated in PMMA matrix, the hardness and elastic modulus increased up to125% and 130%, respectively [151]. Theoretical calculations predict that MoS_2 is mechanically stable and can withstand extra strains with an in-plane stiffness as high as 184 GPa [133]. In the case of graphene–MoS_2–graphene heterostructure the Young's modulus increases almost three times higher than that of single layer MoS_2 theoretically [152]. Some recent studies being carried out here have shown that polymer composites of BCNs exhibit synergy in mechanical properties relative to graphene and BN. Furthermore, graphene can be grafted onto MOFs and other materials to improve their mechanical properties [153].

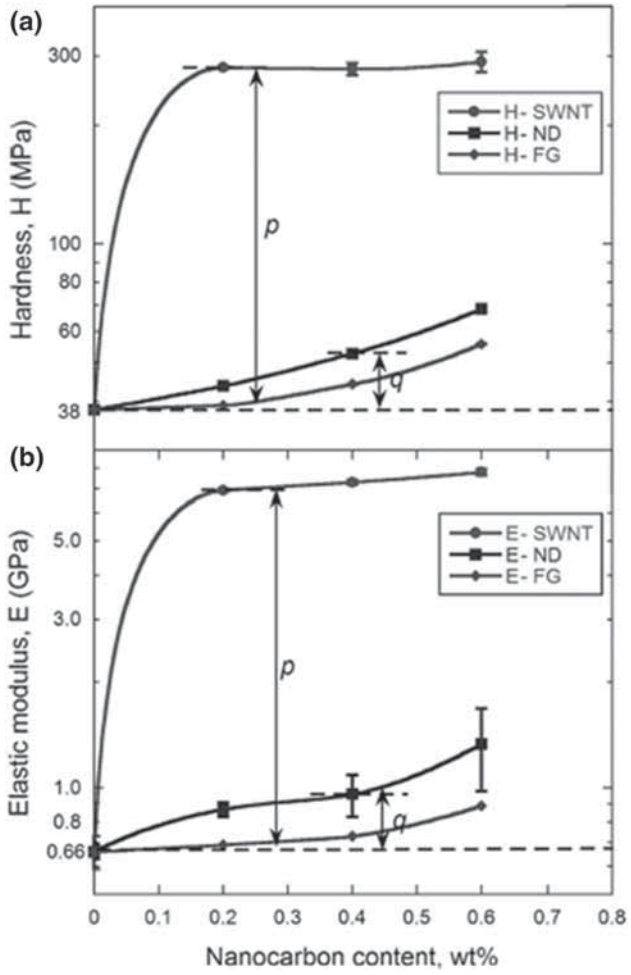

Figure 8. Mechanical properties **(a)** hardness and **(b)** elastic modulus with the variation of nanocarbon content. Single-walled nanotube (SWNT)-reinforced nanocomposites give superior mechanical properties compared with the few-layer graphene (FG) and nanodiamond (ND). Adapted from ref. [150]. Copyright 2009 National Academy of Sciences (USA).

10. Conclusions

The previous sections would suffice to indicate the fascinating properties exhibited by graphene, MoS_2 and other 2D materials. The subject is being pursued widely, and much more will be done in the next few years. This is particularly because of the properties worthy of practical applications. For example, in the HER, MoS_2- and BCN-based materials exhibit excellent activity. Similarly, MoS_2 is useful in fabricating Na-ion batteries with desirable characteristics. We should not forget that graphene itself has found applications in supercapacitors and other areas related to electronic and energy devices. Being a direct band gap material, MoS_2 exhibits unique properties such as intense photoluminescence and circular luminescence. Photoluminescence of single-layer MoS_2 can be used for sensor applications. Optical and electronic properties of MoS_2 and other 2D materials are

indeed very attractive. There are likely to be applications of heterojunctions, covalently cross-linked structures as well as van der Waals structures.

References

[1] Rao C N R, Gopalakrishnan K and Maitra U 2015 *ACS Appl. Mater. Interfaces* **7** 7809

[2] Rao C N R and Waghmare U V 2017 *2D inorganic materials beyond graphene* 476pp

[3] Rao C N R, Gopalakrishnan K and Govindaraj A 2014 *Nano Today* **9** 324

[4] Rao C N R and Gopalakrishnan K 2017 *ACS Appl. Mater. Interfaces* **9** 19478

[5] Rao C N R, Maitra U and Waghmare U V 2014 *Chem. Phys. Lett.* **609** 172

[6] Rao C N R, Pramoda K and Kumar R 2017 *Chem. Commun.* **53** 10093

[7] Rao C N R and Sood A K 2013 *Graphene: synthesis, properties, and phenomena* (Weinheim, Germany: Wiley-VCH)

[8] Novoselov K S, Jiang D, Schedin F, Booth T J, Khotkevich V V, Morozov S V *et al* 2005 *Proc. Natl. Acad. Sci. USA* **102** 10451

[9] Rao C N R, Sood A K, Subrahmanyam K S and Govindaraj A 2009 *Angew. Chem. Int. Ed.* **48** 7752

[10] Subrahmanyam K S, Panchakarla L S, Govindaraj A and Rao C N R 2009 *J. Phys. Chem. C* **113** 4257

[11] Panchakarla L S, Subrahmanyam K S, Saha S K, Govindaraj A, Krishnamurthy H R, Waghmare U V *et al* 2009 *Adv. Mater.* **21** 4726

[12] Wei D, Liu Y, Wang Y, Zhang H, Huang L and Yu G 2009 *Nano Lett.* **9** 1752

[13] Li X, Wang H, Robinson J T, Sanchez H, Diankov G and Dai H 2009 *J. Am. Chem. Soc.* **131** 15939

[14] Kumar N, Moses K, Pramoda K, Shirodkar S N, Mishra A K, Waghmare U V *et al* 2013 *J. Mater. Chem. A* **1** 5806

[15] Smith R J, King P J, Lotya M, Wirtz C, Khan U, De S *et al* 2011 *Adv. Mater.* **23** 3944

[16] Coleman J N, Lotya M, O'Neill A, Bergin S D, King P J, Khan U *et al* 2011 *Science* **331** 568

[17] Joensen P, Frindt R F and Morrison S R 1986 *Mater. Res. Bull.* **21** 457

[18] Eda G, Yamaguchi H, Voiry D, Fujita T, Chen M and Chhowalla M 2011 *Nano Lett.* **11** 5111

[19] Wang S, Rong Y, Fan Y, Pacios M, Bhaskaran H, He K *et al* 2014 *Chem. Mater.* **26** 6371

[20] Shi J, Zhang X, Ma D, Zhu J, Zhang Y, Guo Z *et al* 2015 *ACS Nano* **9** 4017

[21] Feng Q, Zhu Y, Hong J, Zhang M, Duan W, Mao N *et al* 2014 *Adv. Mater.* **26** 2648

[22] Liu K K, Zhang W, Lee Y-H, Lin Y-C, Chang M-T, Su C-Y *et al* 2012 *Nano Lett.* **12** 1538

[23] Gao M-R, Xu Y-F, Jiang J and Yu S-H 2013 *Chem. Soc. Rev.* **42** 2986

[24] Mahler B, Hoepfner V, Liao K and Ozin G A 2014 *J. Am. Chem. Soc.* **136** 14121

[25] Pramoda K, Ayyub M M, Singh N K, Chhetri M, Gupta U, Soni A *et al* 2017 *J. Phys. Chem. C* https://doi.org/10.1021/acs.jpcc.7b10782

[26] Pramoda K, Gupta U, Chhetri M, Bandyopadhyay A, Pati S K and Rao C N R 2017 *ACS Appl. Mater. Interfaces* **9** 10664

[27] Castro Neto A H, Guinea F, Peres N M R, Novoselov K S and Geim A K 2009 *Rev. Modern Phys.* **81** 109

[28] Fang T, Konar A, Xing H and Jena D 2008 *Phys. Rev. B* **78** 205403

[29] Daeha J, Chunder A, Lei Z and Saiful I K 2010 *Nanotechnology* **21** 165202

[30] Fiori G, Betti A, Bruzzone S and Iannaccone G 2012 *ACS Nano* **6** 2642

[31] Sreedhara M B, Gopalakrishnan K, Bharath B, Kumar R, Kulkarni G U and Rao C N R 2016 *Chem. Phys. Lett.* **657** 124

[32] Jena D 2013 *Proc. IEEE* **101** 1585

[33] Schwierz F, Pezoldt J and Granzner R 2015 *Nanoscale* **7** 8261

[34] Chhowalla M, Shin H S, Eda G, Li L-J, Loh K P and Zhang H 2013 *Nat. Chem.* **5** 263

[35] Ayari A, Cobas E, Ogundadegbe O and Fuhrer M S 2007 *J. Appl. Phys.* **101** 014507

[36] Late D J, Liu B, Matte H S S R, Dravid V P and Rao C N R 2012 *ACS Nano* **6** 5635

[37] Radisavljevic B, Radenovic A, Brivio J, Giacometti V and Kis A 2011 *Nat. Nanotechnol.* **6** 147

[38] Chen F, Xia J, Ferry D K and Tao N 2009 *Nano Lett.* **9** 2571

[39] Konar A, Fang T and Jena D 2010 *Phys. Rev. B* **82** 115452

[40] Jena D and Konar A 2007 *Phys. Rev. Lett.* **98** 136805

[41] Yoon Y, Ganapathi K and Salahuddin S 2011 *Nano Lett.* **11** 3768

[42] Radisavljevic B, Whitwick M B and Kis A 2011 *ACS Nano* **5** 9934

[43] Zhang Y, Ye J, Matsuhashi Y and Iwasa Y 2012 *Nano Lett.* **12** 1136

[44] Britnell L, Gorbachev R V, Jalil R, Belle B D, Schedin F, Mishchenko A *et al* 2012 *Science* **335** 947

[45] Sarkar D, Xie X, Liu W, Cao W, Kang J, Gong Y *et al* 2015 *Nature* **526** 91

[46] Novoselov K S, Geim A K, Morozov S V, Jiang D, Zhang Y, Dubonos S V *et al* 2004 *Science* **306** 666

[47] Yuan W and Shi G 2013 *J. Mater. Chem. A* **1** 10078

[48] Wehling T O, Katsnelson M I and Lichtenstein A I 2009 *Chem. Phys. Lett.* **476** 125

[49] Schedin F, Geim A K, Morozov S V, Hill E W, Blake P, Katsnelson M I *et al* 2007 *Nat. Mater.* **6** 652

[50] Hwang S, Lim J, Park H G, Kim W K, Kim D H, Song I S *et al* 2012 *Curr. Appl. Phys.* **12** 1017

[51] Yoon H J, Jun D H, Yang J H, Zhou Z, Yang S S and Cheng M M C 2011 *Sens. Actuators B: Chem.* **157** 310

[52] Rumyantsev S, Liu G, Shur M S, Potyrailo R A and Balandin A A 2012 *Nano Lett.* **12** 2294

[53] Berdan R, Prodromakis T, Salaoru I, Khiat A and Toumazou C 2012 *App. Phys. Lett.* **101** 243502

[54] Dua V, Surwade S P, Ammu S, Agnihotra S R, Jain S, Roberts K E *et al* 2010 *Angew. Chem. Int. Ed.* **49** 2154

[55] Bi H, Yin K, Xie X, Ji J, Wan S, Sun L *et al* 2013 *Sci. Rep.* **3** 2714

[56] Yuan W, Liu A, Huang L, Li C and Shi G 2013 *Adv. Mater.* **25** 766

[57] Shao Y, Wang J, Wu H, Liu J, Aksay I A and Lin Y 2010 *Electroanalysis* **22** 1027

[58] Zhou M, Zhai Y and Dong S 2009 *Anal. Chem.* **81** 5603

[59] He Q, Sudibya H G, Yin Z, Wu S, Li H, Boey F *et al* 2010 *ACS Nano* **4** 3201

[60] Sudibya H G, He Q, Zhang H and Chen P 2011 *ACS Nano* **5** 1990

[61] Dubovik T V, Itsenko A I, Dolinskaya L P, Zyatkevich N S and Levkov L Y 1995 *Powder Met. Met. Ceram.* **33** 100

[62] Pramoda K, Moses K, Maitra U and Rao C N R 2015 *Electroanalysis* **27** 1892

[63] Li H, Wu J, Yin Z and Zhang H 2014 *Acc. Chem. Res.* **47** 1067

[64] Late D J, Huang Y-K, Liu B, Acharya J, Shirodkar S N, Luo J *et al* 2013 *ACS Nano* **7** 4879

[65] Zhu C, Zeng Z, Li H, Li F, Fan C and Zhang H 2013 *J. Am. Chem. Soc.* **135** 5998

[66] Zhang Y, Zheng B, Zhu C, Zhang X, Tan C, Li H *et al* 2015 *Adv. Mater.* **27** 935

[67] Graf M, Liu K, Sarathy A, Leburton J P and Radenovic A 2017 *Biophys. J.* **114** 180

[68] Lim S, Kang B, Kwak D, Lee W H, Lim J A and Cho K 2012 *J. Phys. Chem. C* **116** 7520

[69] Perkins F K, Friedman A L, Cobas E, Campbell P M, Jernigan G G and Jonker B T 2013 *Nano Lett.* **13** 668

[70] Nair R R, Blake P, Grigorenko A N, Novoselov K S, Booth T J, Stauber T *et al* 2008 *Science* **320** 1308

[71] Wang F, Zhang Y, Tian C, Girit C, Zettl A, Crommie M *et al* 2008 *Science* **320** 206

[72] Chitara B, Panchakarla L S, Krupanidhi S B and Rao C N R 2011 *Adv. Mater.* **23** 5419

[73] Chitara B, Krupanidhi S B and Rao C N R 2011 *App. Phys. Lett.* **99** 113114

[74] Lee H S, Min S-W, Chang Y-G, Park M K, Nam T, Kim H *et al* 2012 *Nano Lett.* **12** 3695

[75] Rao C N R, Matte H S S R and Subrahmanyam K S 2013 *Acc. Chem. Res.* **46** 149

[76] Chou S S, Kaehr B, Kim J, Foley B M, De M, Hopkins P E *et al* 2013 *Angew. Chem. Int. Ed.* **52** 4160

[77] Yin Z, Li H, Li H, Jiang L, Shi Y, Sun Y *et al* 2012 *ACS Nano* **6** 74

[78] Lopez-Sanchez O, Lembke D, Kayci M, Radenovic A and Kis A 2013 *Nat. Nanotechnol.* **8** 497

[79] Jariwala D, Marks T J and Hersam M C 2016 *Nat. Mater.* **16** 170

[80] Freitag M, Low T, Xia F and Avouris P 2012 *Nat. Photon.* **7** 53

[81] Wang X, Cheng Z, Xu K, Tsang H K and Xu J-B 2013 *Nat. Photon.* **7** 888

[82] Yan J, Kim M H, Elle J A, Sushkov A B, Jenkins G S, Milchberg H M *et al* 2012 *Nat. Nanotechnol.* **7** 472

[83] Britnell L, Ribeiro R M, Eckmann A, Jalil R, Belle B D, Mishchenko A *et al* 2013 *Science* **340** 1311

[84] Baugher B W H, Churchill H O H, Yang Y and Jarillo-Herrero P 2014 *Nat. Nanotechnol.* **9** 262

[85] Lee C-H, Lee G-H, van der Zande A M, Chen W, Li Y, Han M *et al* 2014 *Nat. Nanotechnol.* **9** 676

[86] Kotz R and Carlen M 2000 *Electrochim. Acta* **45** 2483

[87] Zhang L L and Zhao X S 2009 *Chem. Soc. Rev.* **38** 2520

[88] Vivekchand S R C, Rout C S, Subrahmanyam K S, Govindaraj A and Rao C N R 2008 *J. Chem. Sci.* **120** 9

[89] Stoller M D, Park S, Zhu Y, An J and Ruoff R S 2008 *Nano Lett.* **8** 3498

[90] Kim T, Jung G, Yoo S, Suh K S and Ruoff R S 2013 *ACS Nano* **7** 6899

[91] Zhu Y, Murali S, Stoller M D, Ganesh K J, Cai W, Ferreira P J *et al* 2011 *Science* **332** 1537

[92] Zhu Y, Murali S, Stoller M D, Velamakanni A, Piner R D and Ruoff R S 2010 *Carbon* **48** 2118

[93] Yoo J J, Balakrishnan K, Huang J, Meunier V, Sumpter B G, Srivastava A *et al* 2011 *Nano Lett.* **11** 1423

[94] Jeong H M, Lee J W, Shin W H, Choi Y J, Shin H J, Kang J K *et al* 2011 *Nano Lett.* **11** 2472

[95] Wen Z, Wang X, Mao S, Bo Z, Kim H, Cui S *et al* 2012 *Adv. Mater.* **24** 5610

[96] Gopalakrishnan K, Moses K, Govindaraj A and Rao C N R 2013 *Solid State Commun.* **175** 43

[97] Gopalakrishnan K, Govindaraj A and Rao C N R 2013 *J. Mater. Chem. A* **1** 7563

[98] Sun L, Wang L, Tian C, Tan T, Xie Y, Shi K *et al* 2012 *RSC Adv.* **2** 4498

[99] Niu L, Li Z, Hong W, Sun J, Wang Z, Ma L *et al* 2013 *Electrochim. Acta* **108** 666

[100] Zuo Z, Jiang Z and Manthiram A 2013 *J. Mater. Chem. A* **1** 13476

[101] Han J, Zhang L L, Lee S, Oh J, Lee K-S, Potts J R *et al* 2013 *ACS Nano* **7** 19

[102] Peng Z, Ye R, Mann J A, Zakhidov D, Li Y, Smalley P R *et al* 2015 *ACS Nano* **9** 5868

[103] Li S, Wang Z, Jiang H, Zhang L, Ren J, Zheng M *et al* 2016 *Chem. Commun.* **52** 10988

[104] Thirumal V, Pandurangan A, Jayavel R and Ilangovan R 2016 *Synth. Met.* **220** 524

[105] Barua M, Sreedhara M B, Pramoda K and Rao C N R 2017 *Chem. Phys. Lett.* **683** 459

[106] Acerce M, Voiry D and Chhowalla M 2015 *Nat. Nanotechnol.* **10** 313

[107] Choudhary N, Patel M, Ho Y-H, Dahotre N B, Lee W, Hwang J Y *et al* 2015 *J. Mater. Chem. A* **3** 24049

[108] Cao L, Yang S, Gao W, Liu Z, Gong Y, Ma L *et al* 2013 *Small* **9** 2905

[109] da Silveira Firmiano E G, Rabelo A C, Dalmaschio C J, Pinheiro A N, Pereira E C, Schreiner W H *et al* 2014 *Adv. Energy Mater.* **4** 1301380

[110] Gopalakrishnan K, Pramoda K, Maitra U, Mahima U, Shah M A and Rao C N R 2015 *Nanomater. Energy* **4** 9

[111] Bissett M A, Kinloch I A and Dryfe R A W 2015 *ACS Appl. Mater. Interfaces* **7** 17388

[112] Qu L, Liu Y, Baek J-B and Dai L 2010 *ACS Nano* **4** 1321

[113] Shao Y, Zhang S, Engelhard M H, Li G, Shao G, Wang Y *et al* 2010 *J. Mater. Chem.* **20** 7491

[114] Liu M, Song Y, He S, Tjiu W W, Pan J, Xia Y Y *et al* 2014 *ACS Appl. Mater. Interfaces* **6** 4214

[115] Fu X, Jin J, Liu Y, Wei Z, Pan F and Zhang J 2014 *ACS Appl. Mater. Interfaces* **6** 3930

[116] Vikkisk M, Kruusenberg I, Joost U, Shulga E, Kink I and Tammeveski K *Appl. Catal. B: Environ.* **147** 369

[117] Zhang L and Xia Z 2011 *J. Phys. Chem. C* **115** 11170

[118] Moses K, Kiran V, Sampath S and Rao C N R 2014 *Chem. Asian J.* **9** 838

[119] Wang S, Zhang L, Xia Z, Roy A, Chang D W, Baek J-B *et al* 2012 *Angew. Chem. Int. Ed.* **51** 4209

[120] Sheng Z-H, Gao H-L, Bao W-J, Wang F-B and Xia X-H 2012 *J. Mater. Chem.* **22** 390

[121] Xue Y, Yu D, Dai L, Wang R, Li D, Roy A *et al* 2013 *Phys. Chem. Chem. Phys.* **15** 12220
[122] Wang T, Gao D, Zhuo J, Zhu Z, Papakonstantinou P, Li Y *et al* 2013 *Chem. Eur. J.* **19** 11939
[123] Rowley-Neale S J, Fearn J M, Brownson D A C, Smith G C, Ji X and Banks C E 2016 *Nanoscale* **8** 14767
[124] Reddy A L M, Srivastava A, Gowda S R, Gullapalli H, Dubey M and Ajayan P M 2010 *ACS Nano* **4** 6337
[125] Tian L-L, Wei X-Y, Zhuang Q-C, Jiang C-H, Wu C, Ma G-Y *et al* 2014 *Nanoscale* **6** 6075
[126] Sen S, Moses K, Bhattacharyya A J and Rao C N R 2014 *Chem. Asian J.* **9** 100
[127] Haering R R *et al* 1980 *US Patent* **180** 4224390
[128] Feng C, Ma J, Li H, Zeng R, Guo Z and Liu H 2009 *Mater. Res. Bull.* **44** 1811
[129] Sreedhara M B, Gope S, Vishal B, Datta R, Bhattacharyya A J and Rao C N R 2018 *J. Mater. Chem. A* **6** 2302
[130] Chang K and Chen W 2011 *Chem. Commun.* **47** 4252
[131] Deng D, Novoselov K S, Fu Q, Zheng N, Tian Z and Bao X 2016 *Nat. Nanotechnol.* **11** 218
[132] Chhetri M, Maitra S, Chakraborty H, Waghmare U V and Rao C N R 2016 *Energy Environ. Sci.* **9** 95
[133] Peng Q and De S 2013 *Phys. Chem. Chem. Phys.* **15** 19427
[134] Yeh T-F, Syu J-M, Cheng C, Chang T-H and Teng H 2010 *Adv. Funct. Mater.* **20** 2255
[135] Yeh T-F, Cihlář J, Chang C-Y, Cheng C and Teng H 2013 *Mater. Today* **16** 78
[136] Seo B, Jung G Y, Sa Y J, Jeong H Y, Cheon J Y, Lee J H *et al* 2015 *ACS Nano* **9** 3728
[137] Gupta U and Rao C N R 2017 *Nano Energy* **41** 49
[138] Chhetri M, Gupta U, Yadgarov L, Rosentsveig R, Tenne R and Rao C N R 2016 *ChemElectroChem* **3** 1937
[139] Voiry D, Salehi M, Silva R, Fujita T, Chen M, Asefa T *et al* 2013 *Nano Lett.* **13** 6222
[140] Lu Q, Yu Y, Ma Q, Chen B and Zhang H 2016 *Adv. Mater.* **28** 1917
[141] Maitra U, Gupta U, De M, Datta R, Govindaraj A and Rao C N R 2013 *Angew. Chem. Int. Ed.* **52** 13057
[142] Gupta U, Naidu B S, Maitra U, Singh A, Shirodkar S N, Waghmare U V *et al* 2014 *APL Mater.* **2** 092802
[143] Wang L, Liu X, Luo J, Duan X, Crittenden J, Liu C *et al* 2017 *Angew. Chem. Int. Ed.* **129** 7718
[144] Fan W, Lai Q, Zhang Q and Wang Y 2011 *J. Phys. Chem. C* **115** 10694
[145] Li Q, Guo B, Yu J, Ran J, Zhang B, Yan H *et al* 2011 *J. Am. Chem. Soc.* **133** 10878
[146] Zhang W, Li Y, Peng S and Cai X 2014 *Beilstein J. Nanotechnol.* **5** 801
[147] Zong X, Wu G, Yan H, Ma G, Shi J, Wen F *et al* 2010 *J. Phys. Chem. C* **114** 1963
[148] Liu M, Li F, Sun Z, Ma L, Xu L and Wang Y 2014 *Chem. Commun.* **50** 11004
[149] Barun D, Prasad K E, Ramamurty U and Rao C N R 2009 *Nanotechnology* **20** 125705
[150] Prasad K E, Das B, Maitra U, Ramamurty U and Rao C N R 2009 *Proc. Natl. Acad. Sci. USA* **106** 13186
[151] Kiran M S R N, Raidongia K, Ramamurty U and Rao C N R 2011 *Scr. Mater.* **64** 592
[152] Jiang J-W and Park H S 2014 *Appl. Phys. Lett.* **105** 033108
[153] Kumar R, Raut D, Ramamurty U and Rao C N R 2016 *Angew. Chem. Int. Ed.* **128** 7988